Continuously regenerating Diesel Particulate Filters based on ionically conducting ceramics

E. Obeid, L. Lizarraga, M.N. Tsampas, A. Cordier, A. Boréave, M.C. Steil, G. Blanchard, K. Pajot, P. Vernoux

Continuously regenerating Diesel Particulate Filters based on ionically conducting ceramics

E. Obeid [a], L. Lizarraga [a], M.N. Tsampas [a], A. Cordier [b], A. Boréave [a], M.C. Steil [b], G. Blanchard [c], K. Pajot [c], P. Vernoux [a,*]

[a] *Université de Lyon, Institut de Recherches sur la Catalyse et l'Environnement de Lyon, UMR 5256, CNRS, Université Claude Bernard Lyon 1, 2 Avenue A. Einstein, 69626 Villeurbanne, France*
[b] *Laboratoire d'Electrochimie et de Physicochimie des Matériaux et des Interfaces, UMR 5279, CNRS-Grenoble INP-UJF, BP75, 38402 Saint Martin d'Hères, France*
[c] *PSA PEUGEOT CITROËN, Centre technique de Vélizy, Route de Gisy, 78943 Vélizy-Villacoublay, France*

This study reports a mechanistic study of the soot oxidation on Yttria-Stabilized Zirconia (YSZ), a non-reducible oxide with intrinsic bulk oxygen mobility. Temperature-Programmed Oxidation (TPO) and iso-tope exchange experiments demonstrate the key role of bulk oxygen species in the oxidation process. When "intimate" soot/YSZ contact is achieved after in situ carbon deposition via propylene cracking, lat-tice oxygen ions are the predominant species involved in the oxidation reaction. Based on isotopic TPO experiments performed with different oxygen partial pressures in "tight" contact mode and oxygen exchange measurements, it is proposed that the ignition of the soot oxidation on YSZ can be described as a fuel-cell-type electrochemical mechanism at the nanometric scale. The efficiency of this electro-chemical process seems to depend both on the YSZ/soot contact and on the oxygen partial pressure. In addition, YSZ porous membranes were fabricated in order to simulate porous walls of YSZ-based DPFs. These membranes are effective for soot filtering and soot oxidation with oxygen starts at temperatures over 430 °C, in real soot/catalyst contact.

1. Introduction

CO_2 emissions of Diesel vehicles, and more importantly those of Hybrid Diesel Cars (HDC), are significantly reduced as well as their dependence on fossil fuel. However, European standards for Diesel cars restrict the Particulate Matter (PM) emissions by combining a limit number (6.0×10^{11} particulates/km) with a limit mass (5 mg/km) as well as durability of after-treatment system. Since 2011, all new Diesel cars, sold in EU, are equipped with a Diesel Particulate Filter (DPF) to drastically remove soot particulates. DPFs present high filtering efficiency (>99%) but must be periodically regenerated due to soot particles accumulation [1,2]. Active regeneration is a process triggered by fuel post-injection, which is used for increasing the exhaust temperature up to the soot ignition, via exothermic oxidations of unburnt hydrocarbons in the Diesel Oxidation Catalyst (DOC) placed up-stream the DPF. To limit the fuel overconsumption provoked by post-injections, catalysts are used to promote the soot oxidation process, either added in the combustion chamber as liquid additives (Ce, Fe, etc.) [2–7] or deposited in the DPF channels. The former solution, called Fuel Born Catalyst (FBC), allows tight solid/solid interactions which strongly improve the soot oxidation catalytic process at 500 °C [8]. Nevertheless, the FBC process requires investment costs due to the presence of the additives, the tank as well as the dosing pump. In addition, accumulation of ashes can occur in the DPF. Another approach is the continuously regenerating trap (CRT) which uses NO_2 to oxidize the carbonaceous particles. This gas can oxidize soot in a more efficient way and at lower temperatures (usually from 250 °C) than oxygen [9]. Unfortunately, this technology presents the drawback to increase the NO_2/NO_x ratio [10]. In addition, the next EURO 6 standards will require the utilization of a NO_x catalytic after-treatment device [11]. The latter will be preferentially placed between the DOC and the DPF since it is more efficient with a high NO_2/NO_x ratio [12,13]. Therefore, it is uncertain if the required NO_x-to-soot ratio for successful regeneration will be achieved in future engines, making crucial the development of O_2-CRT.

Various families of catalysts have been reported in the literature to be effective for soot oxidation by oxygen. Perovskites [14–16], spinel-types [17,18], and ceria-based oxides [19,20] are the most extensively investigated. The mechanism of soot oxidation with oxygen has been clearly established in the literature that lattice

* Corresponding author. Address: Institut de Recherches sur la Catalyse et l'Environnement de Lyon (IRCELYON), 2 Avenue Albert Einstein, F-69626 Villeurbanne Cedex, France. Fax: +33 4 72431695.
E-mail address: philippe.vernoux@ircelyon.univ-lyon1.fr (P. Vernoux).

oxygen ions of the catalyst are active for soot oxidation, as well as their dependence on the number of active redox sites [19–25]. In addition, soot oxidation predominantly takes place at the particulate/catalyst interface, underlying the crucial importance of the soot/catalyst contact [26–29]. Ceria-based materials exhibit a Mars and Van-Krevelen mechanism [21,23]. The reducibility of ceria (Ce^{4+} into Ce^{3+}) and its high oxygen storage capacity can generate mobile bulk species effective for soot oxidation. Substitution of ceria with various cations can improve their redox properties. For instance, it was shown that a partial substitution of Ce^{4+} by La^{3+} can enhance the catalytic performances for soot oxidation by increasing the reducibility and then the quantity of active lattice oxygen species [21]. Comparing zirconium versus lanthanum substitution in a ceria solid solution, Katta et al. [30] have concluded that La-doped ceria is more active for soot combustion due to the extrinsic oxygen vacancies induced by La^{3+} substitution which improve the oxygen mobility. Aneggi et al. [31] have confirmed that soot particles are oxidized by surface active oxygens donated by different compositions of ceria–zirconia solid solutions. The vacancies induced by the oxidation are refilled by gaseous oxygen and/or subsurface bulk oxygen. Therefore, the activity is linked with the specific surface area (quantity of Ce^{4+} cations on the surface) as well as with the bulk oxygen mobility characterized by the oxygen storage capacity. A dual mechanism seems to occur on ceria-based catalyst coupling a surface redox process (surface oxygen exchange) and a reverse-spillover of bulk oxygen species.

Our technological target is the development of an O_2-assisted CRT, suitable with EURO 6 standards, which will not require either a fuel overconsumption or a noble metal. The idea is to elaborate a DPF using a catalytic material in order to provide sufficient contact points with the soot particles. Yttria-Stabilized Zirconia (YSZ), an O^{2-} ionically conducting ceramic, was selected as the main component of this O^{2-}-assisted CRT because (i) YSZ presents high chemical and thermal stability as demonstrated in sensors (Lambda sensors) and solid oxide fuel cells technologies, up to 1000 °C in both reducing and oxidizing atmospheres, (ii) YSZ powders can be easily sintered and transformed into monolithic devices. Therefore, our objective is to develop a YSZ-based O_2-assisted CRT. On the contrary with all oxide catalysts reported in literature for soot combustion [14–25,27,31], YSZ does not present any redox properties in Diesel exhaust conditions (oxygen excess). Indeed, neither Zr^{4+}, nor Y^{3+} can change their oxidation states. However, YSZ is known to be an intrinsic O^{2-} conductor due to the presence oxygen vacancies inside its crystallographic structure. The first part of this study demonstrates the catalytic performances of YSZ powder (using different contacts soot/catalyst) for soot combustion. The catalytic mechanism which initiates soot oxidation on this non-reducible oxide has been studied by Temperature-Programmed Oxidation (TPO) with labeled O_2. In the second part, porous YSZ membranes were developed to simulate the porous walls of YSZ-based DPFs. Their filtering and catalytic properties were investigated in quasi real conditions.

2. Materials and methods

2.1. Soot particles production

PM was produced by using a mini Combustion Aerosol Standard (mini-CAST, Jing Ltd., Switzerland) which was used as soot generator. Soot particle size distribution was measured using a SMPS (Model 3080, TSI Inc., St. Paul, MN, USA) with a differential mobility analyzer (DMA) (TSI, Model 3081) column and condensation particle counter (CPC) (TSI, Model 3772). It was operated with a sheath flow of 4 L min^{-1} and an aerosol flow of 0.3 L min^{-1}. The particle diameter scanning was from 12.4 to 562 nm, and each scan required 3 min. The mini-CAST soot generator produces soot particles with physical and chemical properties similar to those of diesel engines. It allows controlling size and chemical composition in a wide range. The generator uses a laminar diffusion flame and consists of an inner burner gas flow and an outer sheath air flow. Oxygen is transported by diffusion from the sheath flow, oxidizing the fuel gas. The flame is "cut open" at halfway to its tip, using N_2 (Linde Gaz, 99.9995%) for quenching the reaction and stabilizing the formed soot particles. Propane (Air Liquide, 99.9995%) was used as fuel, and filtered compressed air was used as sheath gas flow. The mini-CAST was operated at a propane flow of 0.06 L min^{-1} and an air sheath flow of 1.55 L min^{-1}. The N_2 flow for quenching the flame was 7.5 L min^{-1}. After soot particle formation, an air dilution flow of 6.2 L min^{-1} was fixed inside the mini-CAST to obtain a total flow of 15 L min^{-1} at the outlet. Soot generated from the mini-CAST under these conditions presented a size particle distribution centered at around 80 nm with a maximal concentration at 4×10^8 particles/cm^3. Although the quantity was higher, the size distribution was similar to that given by diesel engines [32,33]. Besides, Ferge et al. [34] reported a similar EC (Elemental Carbon)/TC (Total Carbon) ratio (~0.95) for PM emitted from a diesel engine and from a mini-CAST under similar conditions to those used in the present work. SEM and TEM images of soot obtained from this mini-CAST in the mentioned working conditions show a similar morphology and microstructure with diesel engine soot [35]. Thus, soot generated by the mini-CAST is a good proxy for diesel PM. The reactivity of this CAST soot was compared with that of the Printex U model soot (purchased from Degussa), which was widely used in previous studies [19–21,26,36,37].

2.2. YSZ physical and chemical characterizations

Yttria-Stabilized Zirconia (YSZ) powder, containing 8 mol% of yttria from TOSOH, $(ZrO_2)_{0.92}(Y_2O_3)_{0.08}$, was used as purchased. The BET surface area and the pore volume (BJH method) were measured employing nitrogen physisorption at −196 °C using a Micromeritics Tristar. The morphology of the YSZ powder was observed by SEM (Hitachi S800 FEG) applying an acceleration voltage of 15 kV. The samples were deposited on a carbon self-adhesive tape that was then stuck on an aluminum holder and coated by a gold film using cathodic pulverization. In addition, the distribution in size of the YSZ grains was measured by using the laser granulometry technique. XRD patterns were performed on a powder X-ray diffractometer (aD8A25 Brucker) using Cu Kα (λ = 0.15406 nm) radiation and a graphite back-monochromator. Patterns were recorded for 2° values comprised between 10° and 80° by a 0.02° step, with step duration of 94.5 s. The possible presence of chemical impurities (Cl, Na, S, Al, Ti, Si) was analyzed by using a ICP–OES Horiba Jobin Yvon Activa apparatus. The YSZ powder was previously dissolved by an acidic attack.

High-resolution transmission electron microscopy (TEM) was achieved with a JEOL 2010 LaB6 microscope. The acceleration voltage was 200 kV with LaB6 emission current and the point resolution was 0.19 nm. The samples were previously dispersed in isopropanol using ultrasonic bath. One drop at the surface of this suspension was sampling and then deposited on holey carbon coated 200 mesh, Cu, PK/100 grid.

The surface Zr^{4+}/Y^{3+} ratio was determined by X-ray photoelectron spectrometry (XPS, Kratos Ultra DLD spectrometer) using a Al Kα ($h\nu$ = 1486.6 eV) X-ray source. XPS analyses were performed in hybrid mode (magnetic and electrostatic detections) with scanning energy in the analyzer of 20 eV for each element. The binding energies were calibrated using C1S peak of contaminant carbon (BE = 284.6 eV). The Zr atomic percent was determined from the

sum of the areas of Zr 3d5/2 and Zr 3d3/2 peaks using the VISION software (Kratos).

Surface oxygen exchange between gaseous oxygen species ($^{18}O_2$) and bulk YSZ atoms (^{16}O) was carried out at 500 °C. The powder of YSZ (20 mg) was exposed to 1% $^{18}O_2$ in He for 1 h. The different oxygen species, $^{16}O_2$, $^{16}O^{18}O$ and $^{18}O_2$ were analyzed by the VG Gasslab 300 quadrupole mass spectrometer.

2.3. Catalytic performances measurements of YSZ powders

2.3.1. Tests on YSZ/soot mixtures

Catalytic performances of YSZ were performed by using Temperature-Programmed Oxidation (TPO) tests on powder mixtures. Soot was collected from the mini-CAST outlet within a beaker covered with a filter paper. Collected soot was conserved in a desiccator. CAST soot and YSZ powder were mixed with a ratio 1:4 m/m and crushed for 15 min in a mortar in order to improve the soot/YSZ agglomerate contact, denoted as tight contact as commonly reported in the literature [19–21,26,36,37]. TPOs of the soot/YSZ mixtures (25 mg) were carried out in presence of 5% or 1% of $^{18}O_2$ in helium with a heating ramp of 10 °C/min from room temperature to 750 °C in a fixed-bed tubular quartz reactor (internal diameter = 8 mm) with an overall flow of 1.8 L h^{-1}. Reactant mixtures were monitored with mass flow controllers (Bronkhorst El Flow select with an accuracy better than 1%) using $^{18}O_2$ (Euriso-top, 97.95% ^{18}O, 1.54% ^{16}O and 0.51% ^{17}O, 99.999% purity) and He (Linde Gas, 99.995% purity). The isotopic combustion products were analyzed in the gas stream by a VG Gasslab 300 quadrupole mass spectrometer. Signals at m/z 28, 30, 44, 46, 48 amu corresponding to $C^{16}O$, $C^{18}O$, $C^{16}O_2$, $C^{16}O^{18}O$ and $C^{18}O_2$, respectively, were recorded during the heating ramp. Calibrations of the signals at m/z 32 ($^{16}O_2$), 34 ($^{16}O^{18}O$), and 36 ($^{18}O_2$) amu were performed using $^{18}O_2$ in He (Eurisotop, 2.12% O_2) in He containing 97.93% $^{18}O_2$, 0.5% $^{17}O_2$ and 1.57% $^{16}O_2$, 99.999% purity while that of the signal at m/z 28 ($C^{16}O$) and m/z 44 ($C^{16}O_2$) were done with two standard cylinders of $C^{16}O$ in He (1.02% CO in He, Linde gas, 99.999% purity) and $C^{16}O_2$ in He (1% $C^{16}O_2$ in He, Linde gas, 99.999% purity), respectively. These calibrations were also used for the signals at m/z 28 ($C^{18}O$), 46 ($C^{16}O^{18}O$), and 48 ($C^{18}O^{18}O$) considering the linearity between these signals as it was experimentally checked for signals at m/z 32, 34, and 36. The proportion in the gas phase of the different isotopic products during TPO was quantified by calculating the ratio between the production rate of the specific isotope and the overall production rate of CO or CO_2. For instance, the $rC^{18}O_2/rCO_2$ ratio gives the fraction of $C^{18}O_2$ in the gas phase, where $rC^{18}O_2$ is the production rate of $C^{18}O_2$ and rCO_2 is the overall production rate of CO_2.

In addition, conventional TPO experiments were performed with 5% $^{16}O_2$ (LINDE gas, 99.995% purity) in helium with a heating ramp of 10 °C/min from room temperature to 750 °C in a fixed-bed tubular quartz reactor (internal diameter = 8 mm) with an overall flow of 8 L h^{-1}. TPO measurements were performed for comparison between CAST soot (5 mg), model Printex U soot (5 mg) and YSZ/CAST soot (20 mg/5 mg) mixture. Using same operating conditions, a series of TPO was carried out on the YSZ/CAST soot mixture for different oxygen partial pressures: 0% (pure He), 0.5%, 1%, and 10%. CO_2 production rates were monitored by using a CO_2 infrared analyzer (HORIBA 3000), while CO production rates were measured using a micro-gas chromatograph (SRA 3000).

2.3.2. In situ carbon deposition

Carbon produced by propylene cracking (1) was in situ deposited on YSZ surface to produce an "intimate" contact between soot and catalyst. On the contrary of soot particles, propylene can penetrate into the porosity of the YSZ agglomerates (Fig. 4S) and be adsorbed onto the overall surface specific area of the YSZ powder. YSZ powder was exposed to a propylene flow (8000 ppm using He as carrier gas) at 800 °C for 5 min, cooled down to 200 °C still in propylene/He with a ramp of 10 °C min^{-1}, and finally switched to pure He until the room temperature. Products were analyzed with a mass-spectrometer (VG Gaslab). The production of hydrogen at 800 °C was detected as well as the concomitant consumption of propylene. No oxidation products such as CO or CO_2 were detected, confirming the non-reducible behavior of YSZ.

$$C_3H_6 \rightarrow 3C(s) + 3H_2(g) \quad (1)$$

After this in situ carbon deposition step, a TPO experiment was then performed with 5% $^{18}O_2$ in He, following the same procedure described earlier. The propylene cracking protocol was also performed at 800 °C for 5 h without catalyst in the reactor equipped with a fritted quartz support. The as-produced carbon from cracking on the fritted quartz was consecutively oxidized, with the same TPO procedure used for the CAST soot and the Printex U model soot (Fig. 1).

2.3.3. Catalytic performance measurements of YSZ for CO oxidation

The catalytic performance measurements of YSZ for CO oxidation were carried out at atmospheric pressure in a continuous flow quartz reactor. The reaction gases were CO (Linde, 1.02% CO in He) combined with pure O_2 (Linde, 99.997% O_2) and pure He (Linde, 99.997% He) as a carrier gas. The gas composition was controlled by mass flow controllers (Brooks, 5850 TR Series) and was the following: 1000 ppm CO with 5% O_2 and He balance. The overall flow rate was held constant at 8 L h^{-1}. The product gases for the oxidation of CO were analyzed with an online micro-chromatograph (μGC-R3000 SRA instruments). A K-type thermocouple was attached to the reactor at the catalyst bed in order to monitor the temperature during the heat-up period. The entire reactor was placed in a furnace, which was attached to a temperature controller. The sample was heated from 25 to 750 °C at a rate of 10 °C/min.

2.4. Preparation and characterizations of the YSZ porous membranes

The porous membranes were fabricated from a mixture between the YSZ powder and a pore former (cellulose SigmaCell Type50 from Sigma–Aldrich). This mixture, containing 65 vol.% of cellulose, was dispersed in ethanol and homogenized in a TURBULA mixer for 8 h. The suspension was dried overnight at 100 °C and the resulting powder was granulated using a 100 μm polyamide sieve to eliminate large aggregates. The granulated powders were uniaxially pressed under 50 MPa and then isostatically pressed under 100 MPa. The pellets were heated at 50 °C h^{-1} at 500 °C for elimination of cellulose and sintered at 1500 °C for 2 h in air.

The densities and porosities of the samples were measured by mercury porosimetry technique (AUTOPORE 9215). The total porosity obtained was 50% with 47% of open porosity. The pore size distribution was narrow with a mean pore size of 5.8 μm. For the catalytic tests, the samples were machined after sintering by diamond tools into pellets of 16.3 mm in diameter and 1.7 mm in thickness.

The YSZ porous membrane performances (filtering efficiency and catalytic activity) were performed with a bench designed to simulate the exhaust of a diesel engine and described elsewhere [38]. The setup simulated the diesel soot engine using a mini CAST operated at the same conditions than those previously described for soot collection to perform TPO experiments. Gas stream composition was analyzed online using a micro-Gas Chromatograph (R 3000 SRA) to measure light hydrocarbons (CH_4, C_3H_8, etc.), CO, CO_2, O_2, and N_2 concentrations and an Infra-Red analyzers (EMERSON NGA2000) for CO, CO_2, N_2O, and H_2O.

A quartz reactor with two compartments was used to introduce the YSZ porous membranes in the bench line (Fig. 2). The reactor

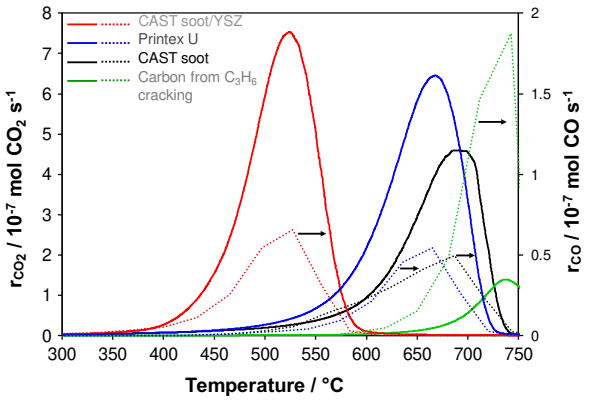

Fig. 1. CO_2 and CO production rates as a function of temperature during the combustion of the CAST soot, the PRINTEX U model soot, the carbon produced by C_3H_6 cracking and the CAST soot mixed with YSZ (tight contact). Reactive mixture: 5% O_2/He, overall flow: 8 L h^{-1}.

consisted of two quartz tubes and a Teflon holder. The inner tube was open in the two edges; one end with an external diameter of 18.5 mm, a little wider than the pellet, and the other suitable to connect it to a ¼′ stainless steel pipeline as outlet of the reactor. The porous pellets were sealed to the inner tube in the widest end (Fig. 2). The inner quartz tube was fixed to the Teflon holder using viton caps. One end of the outer quartz tube acted as reactor inlet (stream from the mini-CAST); the other edge was closed with the Teflon holder using adequate viton caps to ensure the reactor airtightness. The YSZ porous pellet worked as a membrane separating the two reactor compartments. The stream with soot went through the pellet. The quartz reactor was heated by a tubular furnace. A thermocouple chromel–alumel (type K) was used to measure the reactor temperature close to the YSZ porous pellet. The pressure drop values between the reactor's inlet and outlet were measured using a pressure sensor (Keller). A SMPS was used to evaluate the filtering efficiency. The same working conditions, described in the soot particle production, were used to operate the SMPS.

The study of the soot combustion catalytic performance and the filtering efficiency of the YSZ porous membranes were performed in two stages: a first charging soot step and a second regeneration burning soot step. The YSZ porous pellet was charged with soot for 40 min at 25 °C using only a flow of 0.5 L min^{-1} from the total flow of the mini-CAST (15 L min^{-1}). During this step, the pressure drop (ΔP) between the outlet and the inlet of the reactor was recorded, and the SMPS were used to analyze the YSZ porous pellet filtering efficiency. After 40 min of soot charging, the system was purged with an air flow (0.5 L min^{-1} at 25 °C) for 20 min before the

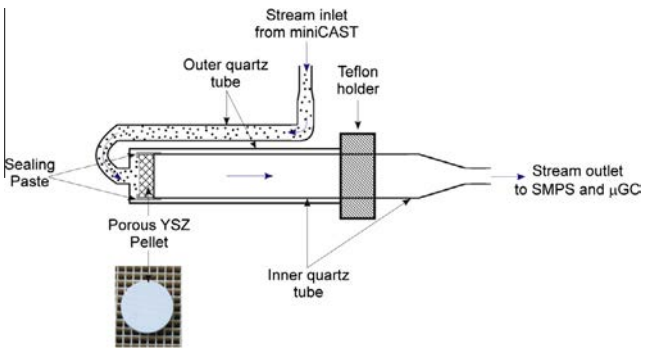

Fig. 2. Scheme of the quartz reactor for YSZ porous membranes filtering efficiency measurements.

regeneration burning soot step starts. The regeneration process consisted in TPO tests carried out to burn soot inside and on the surface of the YSZ porous membrane, previously charged. TPO was performed using a total flow of 0.5 L min^{-1} with different O_2 concentration and N_2 as carrier gas. In the regeneration process, a constant heating rate of 10 °C min^{-1} was used from room temperature to 715 °C. During the TPO, the drop pressure and the gas composition in the reactor outlet were measured.

3. Results and discussions

3.1. YSZ powder characterizations

The YSZ commercial powder was characterized by using different techniques. X-ray diffraction data of the YSZ commercial powder confirm the cubic fluorite structure (Fig. 1S). Textural characterizations display that the powder contained large spherical agglomerates with diameters in the range 20–160 μm (Fig. 2S). The YSZ powder presented a mesoporous behavior with a low BET surface area of 14 m^2 g^{-1} (Fig. 3S, Table 1S). The pores presented a double distribution in size with a predominant centered at around 2.5 nm and a second one at 35 nm (Fig. 4S). Therefore, soot particulates which present a diameter between 30 and 300 nm cannot penetrate into the porosity of the YSZ grains. ICP analysis only revealed the presence of chlorine and sodium (Table 1S), which was not observed on the surface by using XPS. On the opposite, the surface atomic ratio Zr/Y was found to be 4, instead of 5.75 theoretically. This surface segregation of Y has already been observed in literature [39] on similar YSZ powders provided by Tosoh. This indicates that high oxygen vacancies concentration is present on the surface and/or subsurface of YSZ.

3.2. Temperature-programmed oxidation measurements

Fig. 1 shows TPO experiments using 5% O_2 performed on the CAST soot, the Printex U model soot, the propylene cracking carbon and the CAST/soot YSZ mixture (in "tight" contact mode). The soot oxidation for CAST soot, Printex U and carbon produced via propylene cracking took place at high temperature with a maximum of the CO_2 production peak at 683 °C, 665 °C and 734 °C, respectively. These results indicate that the reactivity of the CAST soot is slightly lower than that of the model Printex U soot. The carbon produced from propylene cracking is rather difficult to be oxidized without catalyst as no oxidation process takes place below 600 °C. In addition, its oxidation predominately produces CO. The mixture of the CAST soot with YSZ powder strongly promotes the soot oxidation process as the maximum of the CO_2 production peak shifts from 683 °C to 522 °C, underlying that YSZ is active for soot combustion.

3.3. Isotopic temperature-programmed oxidation of YSZ/soot mixtures

Despite the "loose" contact mode is more representative of the soot/YSZ contact in DPFs, isotopic TPO experiments were performed on YSZ/CAST soot mixtures in "tight" contact mode. Indeed, non-reproducible results have been observed in "loose" contact mode. The variations of the isotopic CO_2 and CO production rates were monitored as a function of temperature for 5% (Fig. 3a) and 1% (Fig. 4a) of $^{18}O_2$ in the gas phase. Soot oxidation starts at around 300 °C in both oxygen partial pressures. Figs. 3b and 4b display the ratios of each isotopic product versus the total CO_2 production during TPO for 5 and 1% of $^{18}O_2$, respectively. The production of CO is low and the CO_2 selectivity is larger than 95% during TPOs using both 1 and 5% O_2. The most important point is that, below 450 °C, i.e., in the temperature domain of the soot combustion ignition, the main soot combustion product is $C^{16}O_2$. The $rC^{16}O_2/rCO_2$

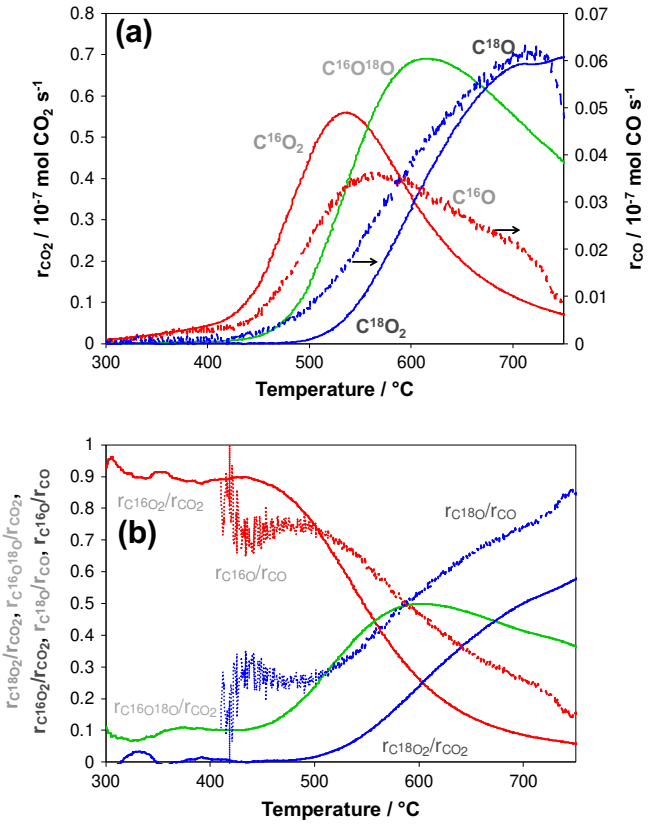

Fig. 3. (a) Isotopic CO_2 and CO production rates and (b) isotopic ratios variations during soot oxidation on YSZ. Reactive mixture: 1% $^{18}O_2$/He.

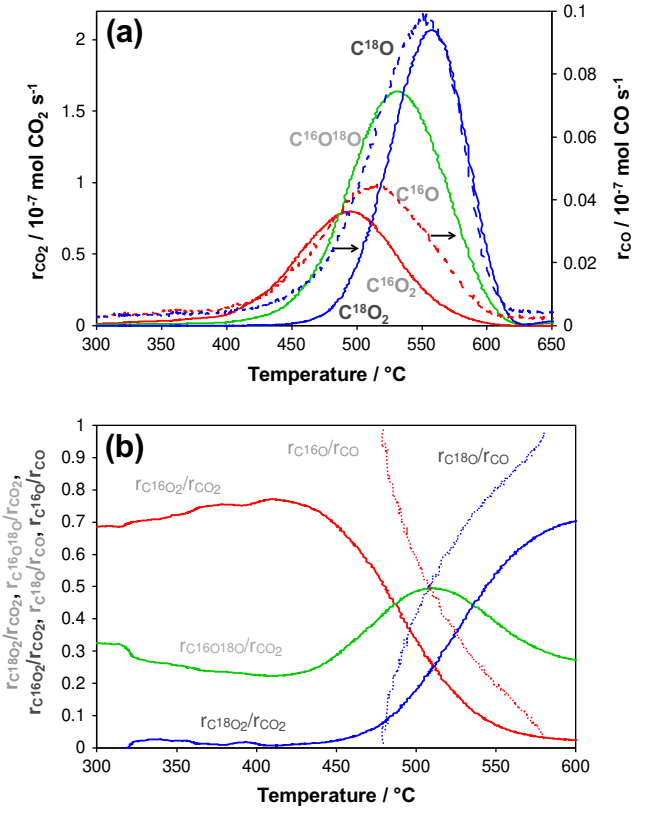

Fig. 4. (a) Isotopic CO_2 and CO production rates and (b) isotopic ratios variations during soot oxidation on YSZ. Reactive mixture: 5% $^{18}O_2$/He.

isotopic ratio was found to be 0.9 with 5% $^{18}O_2$ and between 0.7 and 0.8 for 1% $^{18}O_2$. In addition, in both partial pressures of oxygen, the concentration of $C^{18}O_2$ is negligible in this temperature domain. The production peaks of the different CO_2 products are shifted in temperature. The $C^{16}O_2$ emissions take place first with a peak centered at 533 °C and 492 °C for 1 and 5% of $^{18}O_2$, respectively. Then, the production of $C^{16}O^{18}O$ occurs (peak centered at 614 and 531 °C for 1% and 5% $^{18}O_2$, respectively) followed by a late release of $C^{18}O_2$ (peak at temperature larger than 750 °C with 1% $^{18}O_2$ and centered at 558 °C for 5% $^{18}O_2$). Similar trends are observed for the CO production with a first peak composed of $C^{16}O$ (centered at 562 °C and 513 °C for 1 and 5% of $^{18}O_2$, respectively), followed by a second one of $C^{18}O$ (centered at 715 °C and 550 °C for 1 and 5% of $^{18}O_2$, respectively). All these results underline the higher reactivity, at low temperatures, for soot oxidation of $^{16}O^{2-}$ lattice ions in comparison with the gaseous oxygen species ($^{18}O_2$). Nevertheless, when lowering the oxygen partial pressure in the gas phase, the rate of CO_2 production is decreased in spite of the fact that gaseous oxygen (i.e., $^{18}O_2$) is not effective to oxidize soot particles below 450 °C. This indicates a non-direct impact of the oxygen partial pressure on the soot combustion rate. From $C^{16}O_2$, $C^{16}O$ and $C^{16}O^{18}O$ production peaks, we have calculated the quantity of ^{16}O atoms, i.e., coming from the YSZ catalyst, involved in the soot oxidation process during the overall TPO experiments, up to 750 °C. This amount corresponds to 60% of the total bulk oxygen species initially contained into 20 mg of the YSZ sample (for 5% O_2). This demonstrates that YSZ bulk oxygen species are more active than gaseous oxygen to burn soot, as already observed in literature for reducible oxides [19–25]. Furthermore, bulk oxygen species, and not only surface or subsurface ones, are consumed during soot oxidation. As YSZ is not a reducible oxide, this process gradually replaces $^{16}O_{YSZ}$ atoms utilized for soot oxidation with labeled oxygen atoms (^{18}O) coming from the gas phase. This surface oxygen exchange process explains the secondary cross-labeled production observed during TPO (Figs. 3 and 4) as well as a part of the late emission of non-labeled $C^{18}O_2$. This assumption was confirmed by an isothermal labeled experiment performed at 390 °C with 5% $^{18}O_2$ (Fig. 5S). It is possible to observe (Figs. 3 and 4) that the surface oxygen exchange rate increases with the partial pressure of oxygen as the $rC^{16}O^{18}O/rCO_2$ ratio is higher below 500 °C for 5% $^{18}O_2$. For instance, at 450 °C, the value of the $rC^{16}O^{18}O/rCO_2$ ratio is 0.1 and 0.3 for 1% and 5% $^{18}O_2$, respectively.

In order to investigate the oxygen exchange in absence of soot, YSZ was exposed to 1% $^{18}O_2$ for 1 h at 500 °C (Fig. 5). Only 0.5% of the introduced $^{18}O_2$ was exchanged after 1 h in contrast to 26% exchanged after 1 h during the isothermal oxidation experiment of soot/YSZ mixture conducted at 390 °C (Fig. 5S) or with 60% during

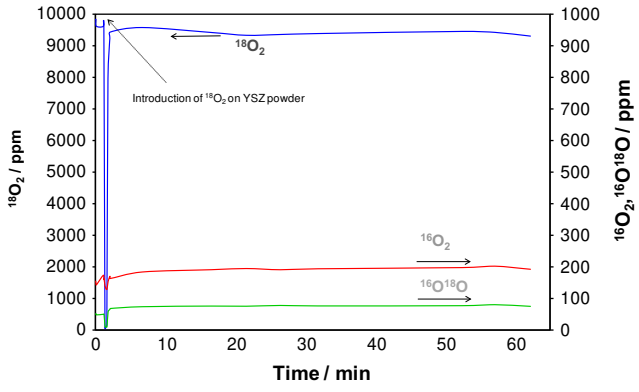

Fig. 5. $^{18}O_2$ oxygen exchange at 500 °C on YSZ. Reactive mixture: 1% $^{18}O_2$/He, overall flow: 1, 8 L h^{-1}.

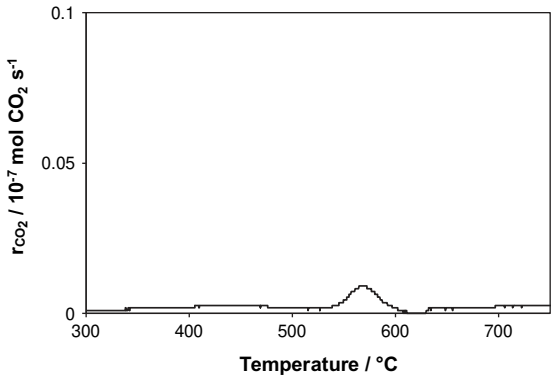

Fig. 6. CO_2 and CO production versus temperature during soot oxidation on YSZ without the presence of oxygen in the gas phase. Desorption in He (8 L h^{-1}), heating ramp = 10 °C min^{-1}.

TPO (Fig. 4). This suggests that soot particulates in contact with YSZ grains promote the surface oxygen exchange.

It was shown that, without the presence of oxygen in the gas phase, soot oxidation did not take place (Fig. 6). We only observed an extremely small production of CO_2 at high temperatures. CO production was not detected during this TPO experiment. However, the upper detection limit of the gas micro-chromatograph is 5 ppm and the maximum CO_2 production was only 10 ppm. This result emphasizes that YSZ bulk oxygen species can only oxidize soot particulates if oxygen is present in the gas phase. This can be explained by the non-redox behavior of YSZ. As far as one bulk oxygen ion is used to oxidize soot, one gaseous oxygen atom must be simultaneously incorporated into YSZ.

3.4. Temperature-programmed oxidation of propylene cracking carbon on YSZ powder

Isotopic TPO measurements were carried out on the YSZ powder after propylene cracking. Fig. 7 shows the isotopic CO_2 and CO production rate as a function of the temperature on YSZ for 5% $^{18}O_2$ in He as carbon was previously deposited over YSZ powder through propylene cracking. CO_2 and CO are produced by the oxidation of the carbon film which covered the overall YSZ surface specific area. The carbon oxidation starts from 170 °C, i.e., 100 °C lower than the soot particles. The most important result is that the main part of the CO_2 and CO productions, between 170 °C and 500 °C, is predominantly composed of $C^{16}O_2$ and $C^{16}O$. Around

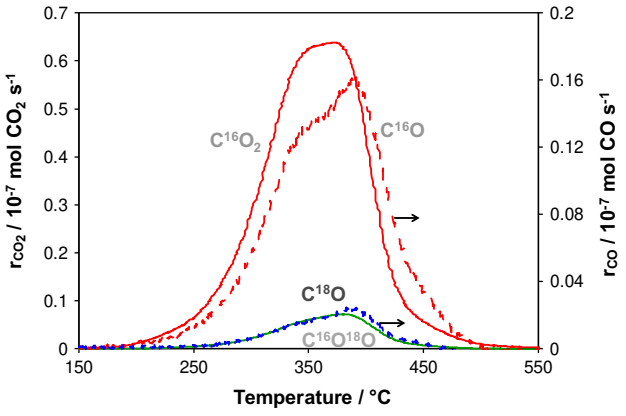

Fig. 7. Isotopic CO_2 and CO production rate variations as a function of the temperature after propylene cracking on YSZ. Reactive mixture: 5% $^{18}O_2$/He.

99% of oxygen species involved in the carbon oxidation process is $^{16}O^{2-}$ anions, i.e., coming from the YSZ surface, subsurface, and bulk. The quantity of carbon produced during the propylene cracking at 800 °C was estimated from the overall CO_2 production. It was found that only 0.93 mg of carbon was in situ generated. This explains the small values of CO_2 production rates compared to those observed with the mixtures YSZ/soot (Fig. 4a) which contained around 5 mg of soot. TEM images were captured to characterize the soot or carbon interface with YSZ powder. Unfortunately, Fig. 8a and b displays that the preparation of the sample (the samples were previously dispersed in isopropanol using ultrasonic bath) for TEM observations can dislocate the YSZ powder (Fig. 2S) to obtain smaller grains of few hundred nanometers. Nevertheless, without this specific preparation, YSZ agglomerates are too thick to be observed with TEM. Then, even if the TEM observations are not fully representative of the real soot/YSZ mixture, they give insights of the interface soot/YSZ. Fig. 8a and c display a TEM image of YSZ before and after the propylene cracking. The observation of the 2 images clearly confirms that the thin coat on YSZ is entirely carbon deposit. In addition, Fig. 8b and c compare a mechanical mixture between soot particles and YSZ with a carbon film in situ deposited on YSZ surface. They clearly show that, in the first case, spherical soot particles (30–100 nm) are organized in the form of grapes which are randomly in contact with YSZ fragments. On the other hand, the thin carbon film (2–5 nm) homogenously covers the YSZ surface. This intimate contact probably explains why 99% of the carbon is oxidized by bulk YSZ oxygen species below 500 °C. This propylene cracking protocol is a powerful tool for investigating the activity of catalyst without contact soot/catalyst limitations. These results underline and confirm the strong impact of the contact area between the catalyst and the soot particulates on the catalytic oxidation efficiency with oxygen [26].

3.5. Mechanism consideration

Isotopic TPO experiments emphasize the key role of bulk oxygen species in the oxidation process. As experimentally investigated (Figs. 3, 4 and 7), the ignition of the soot combustion mainly produces $C^{16}O_2$ and $C^{16}O$, demonstrating that soot reacts with bulk YSZ oxygen species at the contact points. Considering an "intimate" carbon/YSZ contact surface, obtained after in situ carbon deposition via propylene cracking, lattice oxygen ions are the predominant species involved in the overall oxidation process (Fig. 7). To the best of our knowledge, this is the first time that such a result is reported for a non-reducible oxide which presents intrinsic bulk oxygen mobility.

Fig. 9 schematically presents the proposed mechanism for the ignition of the soot oxidation on purely O^{2-} conducting ceramic at low temperatures, i.e., below 500 °C in our case. At higher temperatures, soot oxidation with gaseous oxygen occurs, as suggested by the production of $C^{18}O_2$ (Figs. 3 and 4). From isotopic TPO experiments performed with various oxygen partial pressures and oxygen exchange measurements, we assume that the soot oxidation takes place via a fuel-cell-type electrochemical mechanism at the nanometric scale. The soot oxidation (2) represents the anodic reaction that occurs at the soot/YSZ contact surface. Therefore, the anodic active sites are not in contact with the gas phase, i.e., gaseous oxygen.

$$C + 2\ ^{16}O^{2-}(YSZ) \rightarrow C^{16}O_2(g) + 4\ e^- \quad \text{(through the soot)} \tag{2}$$

$$C + {}^{16}O^{2-}(YSZ) \rightarrow C^{16}O(g) + 2\ e^- \quad \text{(through the soot)} \tag{3}$$

$$C^{16}O + 1/2\,{}^{18}O_2(g) \rightarrow C^{18}O^{16}O(g) \tag{4}$$

$$C^{16}O + {}^{16}O^{2-}(YSZ) \rightarrow C^{16}O_2(g) + 2\ e^- \quad \text{(through the soot)} \tag{5}$$

$$2\ {}^{18}O(ads) + 4\ e^- \quad \text{(through the soot)} \rightarrow 2\ {}^{18}O^{2-}(YSZ) \tag{6}$$

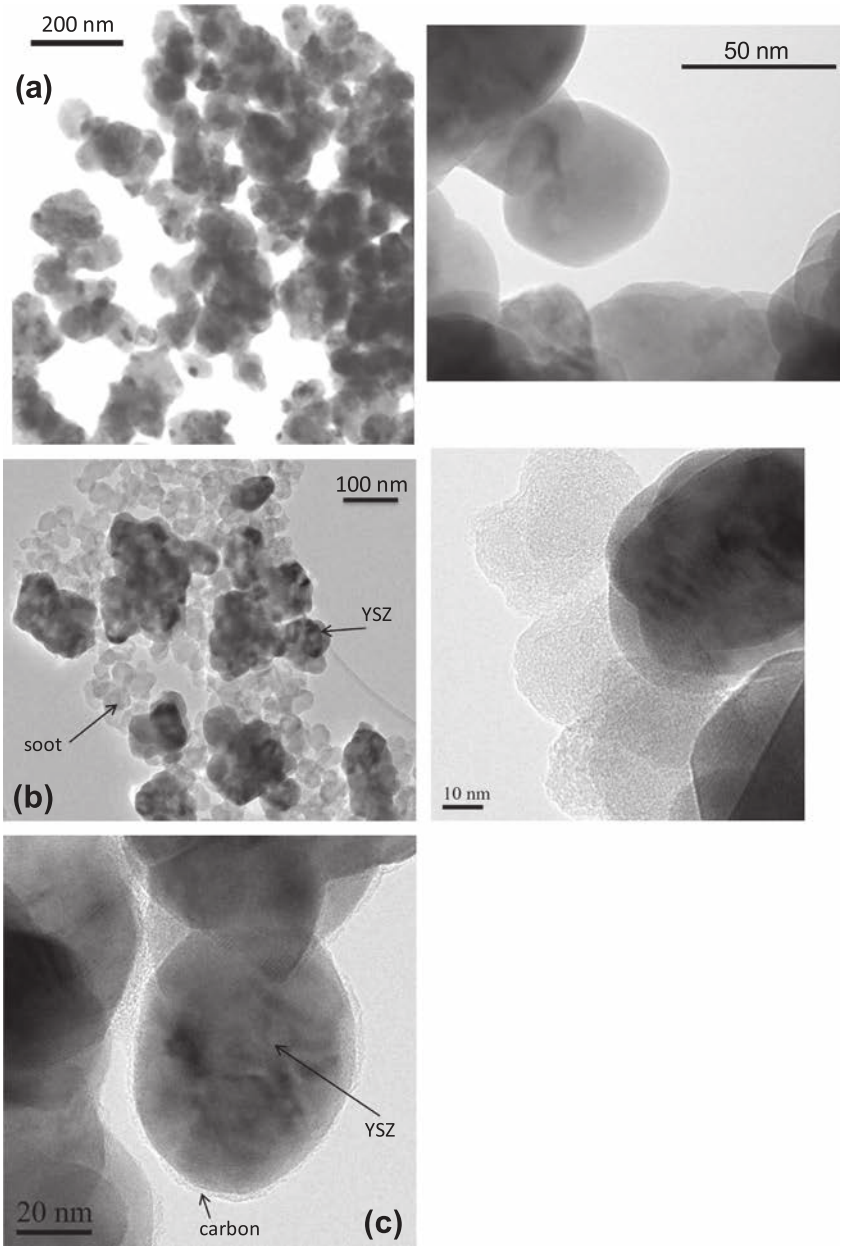

Fig. 8. TEM images of (a) YSZ, (b) the soot particulates and YSZ mixture (after crushing for 15 min in a mortar) and (c) the in situ deposited (after propylene cracking at 800 °C) carbon on YSZ.

Soot electrochemical oxidation can produce CO_2 (2) or CO (3). CO_2 is the predominant product with selectivity larger than 90%. CO can be further oxidize on YSZ by gaseous oxygen (4) or by bulk oxygen species (5) after adsorption on the YSZ surface. Catalytic tests of CO oxidation on YSZ have shown that YSZ can oxidize CO from 300 °C but the CO oxidation rate is low below 450 °C (Fig. 10). In addition, the low production of $C^{18}O^{16}O$ at low temperatures (Figs. 3, 4 and 7) confirms that the reaction (4) is negligible below 500 °C. Nevertheless, reaction (5) cannot be excluded. The electrons produced by the electrochemical oxidation reaction can only diffuse via soot particles which are electronic conductors. Indeed, YSZ is an ionic conductor and exhibits extremely low electronic conductivity lower than 10^{-4} S cm^{-1} in a wide range of oxygen partial pressure between 1 and 10^{-18} atm [40]. Cathodic reactions (6) are expected to take place at the triple phase boundary (tpb) between soot particles, gas phase, and YSZ. Surface oxygen vacancies, in contact with gas-phase oxygen and soot particulates, can dissociatively adsorb oxygen and use electrons coming from the anodes via the soot particles. This fuel-cell-type electrochemical oxidation process is only effective when, as for all fuel cells, an electromotive force is established between the anode and the cathode. This is the case for high oxygen chemical potential gradients between anodic and cathodic points, i.e., for high oxygen partial pressures in the gas phase, as experimentally shown in Fig. 4. Soot particles act both as a reactive and a current collector. This kind of fuel-cell-type electrochemical oxidation process is not possible with ceria-based catalysts since these oxides are also partially electronically conductors due to the Ce^{4+} reduction into Ce^{3+}. Therefore, electrons can path between the anode and the cathode and then inhibit the establishment of an electromotive force, as in solid oxide fuel cells [40].

Fig. 9a and b shows the initial step of the fuel-type soot electrochemical oxidation process with production of $C^{16}O_2$ via direct production of CO_2 (2) or via partial oxidation into CO (3)

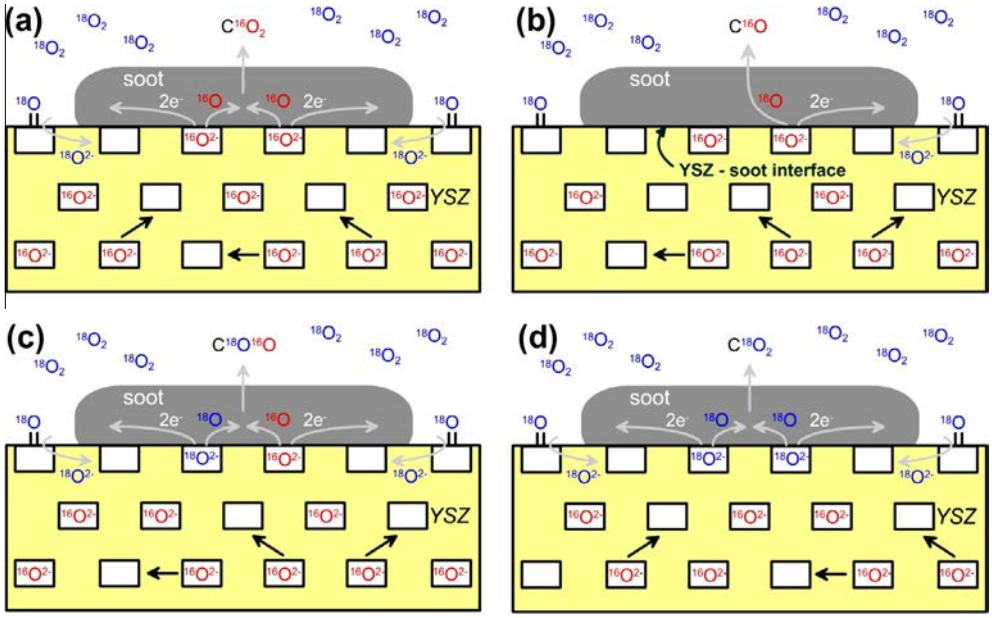

Fig. 9. Schematic drawing of the fuel-cell-type soot electrochemical oxidation on YSZ. (a) Initial step, (b) bulk oxygen ions migration and CO production, (c and d) competition between oxygen ions incorporated at tpb and those coming from the bulk.

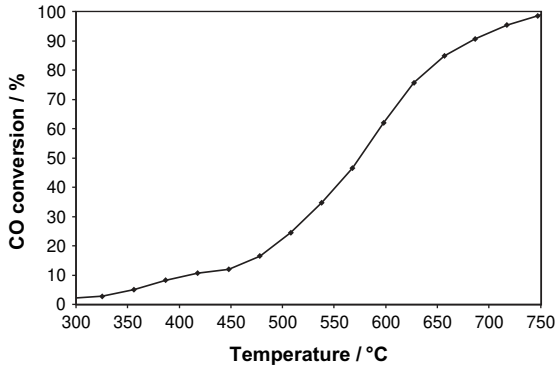

Fig. 10. CO conversion versus temperature on YSZ. Reactive mixture: 1000 ppm CO/ 5% O_2 and He balance, overall flow: at 8 L h^{-1}.

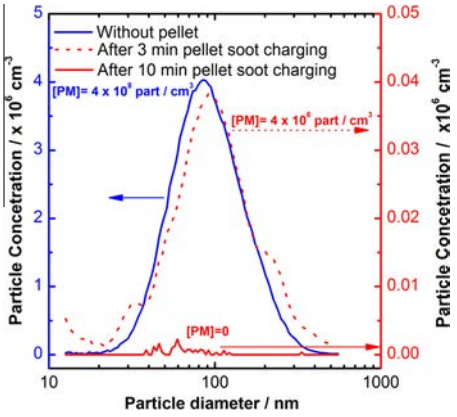

Fig. 11. Soot particle distribution obtained with the SMPS without the YSZ porous membrane (blue solid line); after 3 min of soot loading (red dotted line), and after 10 min of soot loading (red solid line). (For interpretation of the references to colour in this figure legend, the reader is referred to the web version of this article.)

(Figs. 3a and 4a). As YSZ is an oxygen anion conductor, $^{16}O^{2-}$ ions can migrate through the oxygen vacancies in the bulk and reach the soot/YSZ interface (Fig. 9b). At temperatures lower than 400 °C, the ionic conductivity of YSZ is low. Therefore, after few minutes, there is a competition between oxygen ions incorporated at the tpb and those coming from the bulk (Fig. 9c and d), as experimentally observed with the time-shifted production of $C^{16}O^{18}O$ and $C^{18}O_2$ (Figs. 3a and 4a). In addition, an isothermal experiment performed at 390 °C has confirmed this assumption (Fig. 5S). Let us note that when the carbon/YSZ contact is "intimate" (Figs. 7 and 8c), the YSZ domain (most probably the crystallites) directly interfaced with the soot is nanometric (around 50 nm). Therefore, distances of bulk ionic species to reach the soot/catalyst interface are extremely small. The impact of the ionic conductivity becomes negligible and bulk oxygen ionic species are the predominant electroactive species, as experimentally observed (Fig. 7).

3.6. Catalytic performances of YSZ porous membranes

Porous YSZ membranes were prepared in order to simulate porous walls between two channels of a DPF. The catalytic performances for soot oxidation as well as the filtering efficiency of these porous YSZ membranes were evaluated by using a specific reactor (Fig. 2) under a continuous flow of a simulated Diesel exhaust including soot particulates in suspension. Fig. 11 shows the filtering efficiency of YSZ porous membrane, comparing the soot particles size distribution and concentration with and without the YSZ porous membrane in the sampling line. The blue trace shows the soot particles size distribution and concentration for soot particles in the upstream directly generated by the mini-CAST when the membrane was not in the line. After 3 min of soot loading, the particle soot concentration in the downstream of the membrane decreased 2 orders of magnitude (red-dashed trace) compared to the previous case. The soot particle concentration became negligible after 10 min of soot loading (red solid trace). The latter demonstrates the excellent filtering efficiency of the YSZ porous membrane for soot particles. As the YSZ membrane pores become filled by PM, the pressure drop increases together with the filtering efficiency. SEM was used to characterize the contact between soot and YSZ when a porous membrane was loaded with soot particles and cut longitudinally. Fig. 6S shows the SEM image from the pellet side that faced the soot stream during the loading

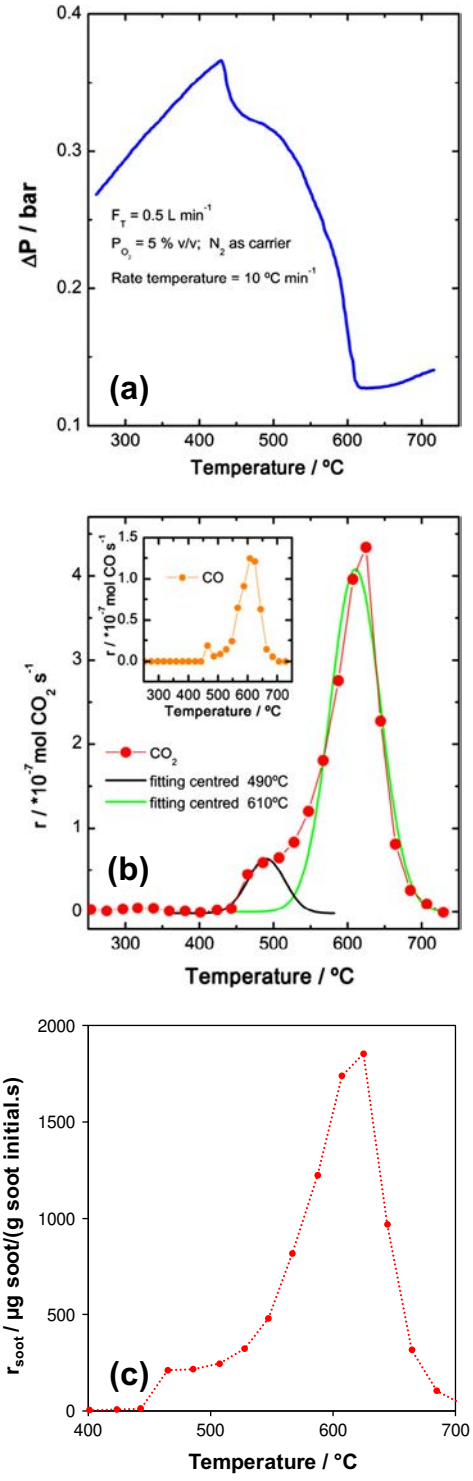

Fig. 12. YSZ porous membrane regeneration process via temperature-programmed oxidation. (a) Pressure drop values (ΔP) as function of the temperature during TPO. (b) Production rate of CO_2 during TPO (red circles), and two Gaussian fitting traces for CO_2 production. Inset: formation rate of CO during TPO. (c) Soot production rare as a function of the temperature. (For interpretation of the references to colour in this figure legend, the reader is referred to the web version of this article.)

process. The image evidences the presence of a thin micrometric soot layer over the YSZ porous pellet surface. As well, soot traces are visible inside the YSZ pellet due to its high porosity.

The CO_2 and CO production rates, expressed in µg of soot/(g of initial soots) [31,41,42], and the pressure drop across the membrane, DP, during the regeneration process as is shown in

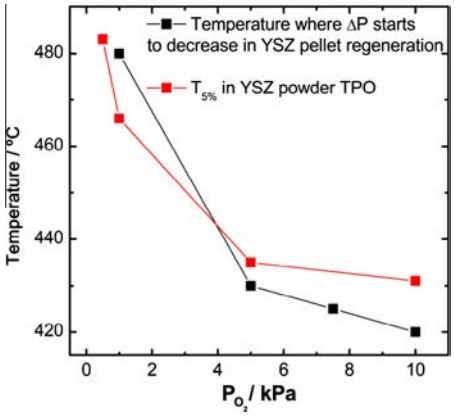

Fig. 13. Comparison of the regeneration steps between YSZ powder and membrane, as a function of the oxygen partial pressure. Black squares: temperatures at which the pressure drop across the membrane started to decrease. Red squares: temperatures at which 5% of soot was burned during TPO of the soot YSZ powder mixture. (For interpretation of the references to colour in this figure legend, the reader is referred to the web version of this article.)

the Fig. 12, presented different stages. The ΔP values linearly increased with temperatures below 430 °C due to the increase of gas viscosity. No detectable formation of CO and CO_2 was observed below 430 °C. From 430 to 615 °C, the pressure drop decreased with temperature; however, three different performances were evidenced in this temperature range: (i) from 430 to 460 °C, the CO_2 and CO production started, and ΔP sharply decreased from 365 to 325 mbar; (ii) from 460 to 515 °C, CO production rate decreased while CO_2 production rate and ΔP values were almost constant. The pressure drop reached a pseudo plateau centered at 320 mbar; (iii) from 515 to 615 °C, CO and CO_2 formation rates reached their maximum values, ΔP decreased again abruptly. After 615 °C, ΔP increased again linearly with temperature (i.e., the gas friction is an increasing function of temperature), whereas CO and CO_2 formation rates decreased and reached zero. It is noticeable in the Fig. 12 that ΔP started to decrease at 430 °C, temperature at which CO and CO_2 formation initiated to be detected. This first pressure drop decrease could be associated with channels opening in the YSZ porous membrane due to soot burning inside its pores. CO and CO_2 production rates show two quasi-Gaussian peaks which in the case of CO_2 are centered at 490 °C and 610 °C. The presence of two quasi-Gaussian traces is indicative of soot burning regeneration being produced by two different phenomena. The peak centered at 610 °C can be attributed to the burning of soot particulates not in a good contact with YSZ since 610 °C is a normal temperature of non-catalyzed soot combustion. This process can occur with soot outside the YSZ pellet, probably accumulated on its surface (Fig. 6S). The peak centered at 490 °C can be related with the combustion of soot particulates in tight contact with YSZ, probably hosted inside the membrane porosity. As soot inside the porous pellet is burned, ΔP sharply decreases. Furthermore, 490 °C is the same temperature value as the first $C^{16}O_2$ production peak shown in Fig. 3a. Soot loading inside the porosity was estimated from the integration of the first peak of CO and CO_2 production rates (490 °C) and was found to be 1.4 g of soot per L of YSZ membrane while the overall soot loading was around 10 g L^{-1}.

Fig. 13 compares the results of YSZ porous membrane regeneration step with the soot TPO using YSZ powder for different oxygen partial pressures. The temperature at which the ΔP started to decrease in the YSZ porous membrane is compared with values of T5 (temperature at which 5% of soot was burned) in the TPO of soot/YSZ mixture. These two parameters exhibit similar values as

well as similar trends as a function of the oxygen partial pressure. The strong oxygen partial pressure dependence of the YSZ catalytic activity for soot combustion is clearly confirmed for both with powder and porous membrane. High oxygen partial pressure values up to 5% are necessary to achieve low regeneration temperatures, at around 430 °C. Regarding the mechanism (Fig. 9), these results indicate that the electrochemical reduction of gaseous oxygen at tpb (6) could be the rate-determining step. Nevertheless, the oxygen partial pressure, in Diesel exhaust, is always larger than 5%, typically in the range 5–10%.

4. Conclusions

This study reports that YSZ can oxidize soot particulates. Isotopic Temperature-Programmed Oxidation (TPO) experiments using labeled oxygen $^{18}O_2$ demonstrate the key role of bulk oxygen species in the oxidation process. Considering an "intimate" soot/YSZ contact surface, obtained after in situ carbon deposition via propylene cracking, lattice oxygen ions are the predominant species involved in the oxidation reaction. To the best of our knowledge, this is the first time that such a result is reported for a non-reducible oxide which presents intrinsic bulk oxygen mobility. From isotopic TPO experiments performed with various oxygen partial pressures in "tight" contact mode and oxygen exchange measurements, we assume that the ignition of the soot oxidation on YSZ involves a fuel-cell-type electrochemical mechanism at the nanometric scale. The efficiency of this electrochemical process seems to depend both on the YSZ/soot contact and on the oxygen partial pressure. YSZ porous membranes were fabricated in order to simulate porous walls of YSZ-based DPFs. These YSZ porous membranes are effective for soot filtering and soot can be oxidized with oxygen from 430 °C.

Acknowledgments

The authors are grateful to the ANR (Agence National de la Recherche) for funding "PIREP2" project (No. ANR-2010-VPTT 006-01) and ADEME (Agence de l'Environnement et de la Maîtrise de l'Energie) for the PhD grant of Emil Obeid.

References

[1] D. Fino, V. Specchia, Powder Technol. 180 (2008) 64–73.
[2] B.A.A.L. van Setten, M. Makkee, J.A. Moulijn, Catal. Rev. 43 (4) (2001) 489–564.
[3] K. Pattas, Z. Samaras, D. Sherwood, K. Umehara, C. Cantiani, O. Aguerre Chariol, Ph. Barthe, J. Lemaire, SAE Technical Paper Series, 1992, 920363.
[4] K. Pattas, N. Kyriakis, E. Vouitsis, T. Manikas, P. Pistikopoulos, Z. Samaras, T. Seguelong, G. Blanchard, SAE Technical Paper Series, 2002, 02FL-92.
[5] O. Savat, P. Marez, G. Belot, SAE Technical Paper, 2000, 2000-01-0473.
[6] G. Blanchard, C. Colignon, C. Griard, C. Rigaudeau, O. Salvet, T. Seguelong, SAE Technical Paper, 2002, 2002-01-2781.
[7] L. Rocher, T. Seguelong, V. Harle, M. Lallemand, M. Pudlarz, M. Macduff, SAE Technical Paper, 2011, 2011-01-0297.
[8] H. Jung, D.B. Kittelson, M.R. Zachariah, Combust. Flame 142 (2005) 276–288.
[9] A. Setiabudi, M. Makkee, J.A. Moulijn, Appl. Catal. B 50 (2004) 185–194.
[10] D.C. Carslaw, Atmos. Environ. 39 (2005) 4793–4802.
[11] P. Granger, V.I. Parvulescu, Chem. Rev. 111 (2011) 3155–3207.
[12] R.Q. Long, R.T. Yang, J. Catal. 207 (2002) 224–231.
[13] I. Malpartida, O. Marie, P. Bazin, M. Daturi, X. Jeandel, Appl. Catal. B 113–114 (2012) 52–60.
[14] D. Fino, N. Russo, G. Saracco, V. Specchia, J. Catal. 217 (2003) 367–375.
[15] N. Russo, D. Fino, G. Saracco, V. Specchia, J. Catal. 229 (2005) 459–469.
[16] M. Sadakane, T. Asanuma, J. Kubo, W. Ueda, Chem. Mater. 17 (2005) 3546–3551.
[17] M. Dhakad, T. Mitshuhashi, S. Rayalu, P. Doggali, S. Bakardjiva, J. Subrt, D. Fino, H. Haneda, N. Labhsetwar, Catal. Today 132 (2008) 188–193.
[18] S. Wagloehner, S. Kureti, Appl. Catal. B 125 (2012) 158–165.
[19] K. Krishna, A. Bueno-Lopez, M. Makkee, J.A. Moulijn, Appl. Catal. B 75 (2007) 189–200.
[20] I. Atribak, A. Bueno-López, A. García-García, J. Mol. Catal. A 300 (2009) 103–110.
[21] A. Bueno-Lopez, K. Krishna, M. Makkee, J.A. Moulijn, J. Catal. 230 (2005) 237–248.
[22] N. Guilhaume, B. Bassou, G. Bergeret, D. Bianchi, F. Bosselet, A. Desmartin-Chomel, B. Jouguet, C. Mirodatos, Appl. Catal. B 119–120 (2012) 287–296.
[23] A. Bueno-López, K. Krishna, B. van der Linden, G. Mul, J.A. Moulijn, M. Makkee, Catal. Today 121 (2007) 237–245.
[24] N. Guillén-Hurtado, A. García-García, A. Bueno-López, J. Catal. 299 (2013) 181–187.
[25] B. Bassou, N. Guilhaume, E.E. Iojoiu, D. Farrusseng, K. Lombaert, D. Bianchi, C. Mirodatos, Catal. Today 159 (2011) 138–143.
[26] J.P.A. Neeft, M. Makkee, J.A. Moulijn, Appl. Catal. B 8 (1996) 57–78.
[27] S.B. Simonsen, S. Dahl, E. Johnson, S. Helveg, J. Catal. 255 (2008) 1–5.
[28] B. Bassou, N. Guilhaume, K. Lombaert, C. Mirodatos, D. Bianchi, Energy Fuels 24 (2010) 4766–4780.
[29] B. Bassou, N. Guilhaume, K. Lombaert, C. Mirodatos, D. Bianchi, Energy Fuels 24 (2010) 4781–4792.
[30] L. Katta, P. Sudarsanam, G. Thrimurthulu, B.M. Reddy, Appl. Catal. B 101 (2010) 101–108.
[31] E. Aneggi, C. de Leitenburg, A. Trovarelli, Catal. Today 181 (2012) 108–115.
[32] C.C. Barrios, A. Dominguez-Saez, J.R. Rubio, M. Pujadas, Aerosol Sci. Technol. 45 (5) (2011) 570–580.
[33] M.R. Canagaratna, J.T. Jayne, D.A. Ghertner, S. Herndon, Q. Shi, J.L. Jimenez, P.J. Silva, P. Williams, T. Lanni, F. Drewnick, K.L. Demerjian, C.E. Kolb, D.R. Worsnop, Aerosol Sci. Technol. 38 (6) (2004) 555–573.
[34] T. Ferge, E. Karg, A. Schroppel, K.R. Coffee, H.J. Tobias, M. Frank, E.E. Gard, R. Zimmermann, Environ. Sci. Technol. 40 (10) (2006) 3327–3335.
[35] M.E. Monge, B. D'Anna, L. Mazri, A. Giroir-Fendler, M. Ammann, D.J. Donaldson, C. George, Proc. Natl. Acad. Sci. USA 107 (15) (2010) 6605–6609.
[36] D. Weng, J. Li, X. Wu, Z. Si, J. Environ. Sci. 23 (1) (2011) 145–150.
[37] I. Atribak, A. Bueno-López, A. García-García, Combust. Flame 157 (2010) 2086–2094.
[38] L. Lizarraga, S. Souentie, A. Boreave, C. George, B. D'Anna, P. Vernoux, Environ. Sci. Technol. 45 (24) (2011) 10591–10597.
[39] J. Zhu, J.G. van Ommen, A. Knoester, L. Lefferts, J. Catal. 230 (2005) 291–300.
[40] E.P. Butler, R.K. Slotwinski, N. Bonanos, J. Drennan, B.C.H. Steele, Science and Technology of Zirconia II, N. Claussen, R. Ruhle, The American Ceramic Society, Westerville, 1984.
[41] B.A.A.L. van setten, J. Bremmer, S.J. Jelles, M. Makkee, J.A. Moulijn, Catal. Today 53 (1999) 613–621.
[42] A. Bueno-López, Appl. Catal. B (2013), http://dx.doi.org/10.1016/j.apcatb.2013.02.033.